

Normal and abnormal electron-hole pairs in a voltage-pulse-driven quantum conductor

X. K. Yue¹ and Y. Yin^{1,*}

¹College of Physical Science and Technology, Sichuan University, Chengdu, Sichuan, 610065, China
(Dated: July 10, 2021)

Electron-hole pairs can be excited coherently in a quantum conductor by applying voltage pulses on its contact. We find that these electron-hole pairs can be classified into two kinds, whose excitation probabilities have different dependence on the Faraday flux of the pulse. Most of the pairs are of the first kind, which can be referred to as “normal” pairs. Their excitation probabilities increase nearly monotonically with the flux and saturate to the maximum value 1 when the flux is large enough. In contrast, there exist “abnormal” pairs, whose excitation probabilities can exhibit oscillations with the flux. These pairs can only be excited by pulses with small width. Due to the oscillation of the probabilities, the abnormal pairs can lead to different features in the full counting statistics of the electron-hole pairs for pulses with integer and noninteger fluxes.

PACS numbers: 73.23.-b, 72.10.-d, 73.21.La, 85.35.Gv

I. INTRODUCTION

The on-demand coherent injection of single or few charges in solid state devices has attracted much attention in the recent decade.^{1–6} In a simple way, such injection can be realized by applying a nanosecond voltage pulse on the Ohmic contact of a quantum conductor at sub-kelvin temperatures, as illustrated in Fig. 1(a). The injected charges are carried by electrons and/or holes in the Fermi sea of the quantum conductor,^{7,8} whose quantum states are well-defined and can be manipulated via the voltage pulse. This setup has been referred to as the voltage pulse electron source, which offers a simple and feasible way to achieve the time-triggered coherent injection.⁹ While a negative pulse tends to inject electrons, a positive pulse tends to inject holes. However, additional electron-hole(eh) pairs can also be excited during the injection, manifesting themselves in the noise of the injected charges.^{10,11}

The statistics of the eh pairs show different features for pulses with integer and noninteger Faraday fluxes. To minimize the noise, pulses with integer fluxes are favorable, since the excitation of the eh pairs are suppressed in this case.¹⁰ Remarkably, the eh pairs can be totally eliminated when the pulse is further tuned to be the form of the Lorentzian.¹² In doing so, one obtains a noiseless current carried by only electrons or holes, whose wave function has a semi-exponential profile in the energy domain.¹ They are now referred to as levitons, which play a central role on the on-demand charge injection.^{9,13,14}

In contrast, a large amount of eh pairs can be excited via pulses with noninteger fluxes. In fact, the number of eh pairs detected over a large time interval t diverges as t increasing, which is closely related to the dynamical orthogonality catastrophe.^{10,15,16} In this case, the quantum states of the eh pairs can show unique features, which can be seen from the interference pattern in the Mach-Zehnder interferometers.¹⁷ Moreover, new types of excitations can be constructed from these states. For example, it has been proposed that, by applying a Lorentzian pulse with one-half flux, a zero-energy quasiparticle with

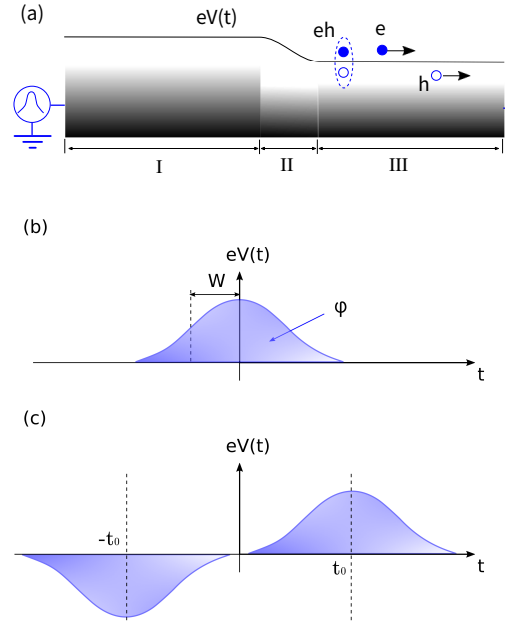


FIG. 1. (a) Schematic of the on-demand charge injection via a voltage pulse $V(t)$. By applying $V(t)$ on the contact of the quantum conductor, electrons (e) and/or holes (h) from the reservoir(region I) can be injected into the quantum conductor(region III), accompanied with additional electron-hole pairs (eh). The voltage drop is assumed to occur across a short interval at the interface(region II). (b) Schematic of the applied voltage pulse. The overall profile of the voltage pulse can be characterized by its half width at half maximum (HWHM) W and Faraday flux ϕ . (c) Schematic of the voltage pulse for electron-hole pair excitation. The two pulses has the same shape but opposite signs.

fractional charge $e/2$ can be created, which is described by a mixed state and cannot exist in the absence of the eh pairs.¹⁸

These studies suggest that the different statistics of the eh pairs can be attributed to their different quantum states. To gain a more comprehensive understanding of such difference, explicit expressions of these quan-

tum states are favorable. However, they are only known for certain specific pulses.^{1,19,20} A general description of these states for arbitrary pulses are still missing, which hinder further developments along this direction.

As a first step toward solving this problem, in this paper we consider the case when two successive pulses with the same shape but opposite signs are applied on the voltage pulse electron source, as illustrated in Fig. 1(c). In this case, the net injected charges are zero and only eh pairs are excited, making it easier to extract their information. For each eh pair, we show that both the excitation probability and the one-body wave function can be obtained from the corresponding scattering matrix of the electron source, which offer a comprehensive description of the quantum states of the eh pairs.

By using such description, we show that all the eh pairs excited by the voltage pulse can be classified into two kinds, despite the detailed shape of the pulse. The excitation probabilities of the two kinds of eh pairs exhibit quite different dependence on the flux of the pulse: For the first kind of eh pairs, their probabilities increase nearly monotonically with the flux. They can saturate to the maximum value 1 when the flux is large enough. Most of the eh pairs belong to this kind, which we refer to as “normal” eh pairs. In contrast, the probabilities for the second kind of eh pairs undergo oscillations with the flux. These pairs can only be excited for pulses with small width, which we here refer to as “abnormal” eh pairs.

We find that the abnormal pairs can play an important role on the full counting statistics (FCS) of the eh pairs. For the voltage pulse electron source, we find that the corresponding FCS can be characterized by an effective binomial distribution, whose cumulant generating function $S(\chi)$ has the form: $S(\chi) = \alpha \ln(1 - \bar{p}_k + e^{i\chi} \bar{p}_k)$, indicating that the electron source can excite effectively α eh pairs with an effective probability \bar{p} . The parameter α *without* and *with* the contribution of the abnormal eh pairs can show qualitatively different behaviors as a function of the flux φ : *Without* the contribution of the abnormal eh pairs, the parameter α exhibits a sequencing of plateaus. The abnormal eh pairs can lead to a derivation from these plateaus, demonstrating the impact of the abnormal eh pairs clearly.

The paper is organized as follows: In Sec. II, we present the model for the voltage pulse electron source and show how to extract the quantum states of the eh pairs from the scattering matrix. In Sec. III, by using a Gaussian-shaped pulse as an example, we show how to classify the two kinds of eh pairs from their excitation probabilities. Their impact on the full counting statistics is also discussed in this section. In Sec. IV, we show that the two kinds of eh pairs can also be found for voltage pulses with different profiles. In particular, we demonstrate how does the abnormal eh pairs evolve when the profile of the pulse approaches the Lorentzian. We summarized in Sec. V.

II. MODEL AND FORMALISM

The voltage pulse electron source can be modeled as a single-mode quantum conductor, where a time-dependent voltage $V(t)$ is applied on the Ohmic contact of the conductor, as illustrated in Fig. 1(a). We assume that $V(t)$ has the form in the time domain

$$V(t) = V_p(t_0 + t) - V_p(t_0 - t), \quad (1)$$

indicating that it is composed of two successive pulses $[\pm V_p(t)]$ with the same shape but opposite signs, which are separated by a time interval t_0 . The width of each pulse can be characterized by the half width at half maximum (HWHM) W , while the strength can be described by the Faraday flux $\varphi = (e/h) \int_{-\infty}^{+\infty} V_p(t) dt$, as illustrated in Fig. 1(b). The time interval t_0 is usually chosen to be larger than the width W of each pulse ($W < t_0$), so that the two pulses are well-separated in time domain, as illustrated in Fig. 1(c).

In the spatial domain, the voltage drop between the contact and the conductor is assumed to occur across a short interval so that the corresponding dwell time τ_D satisfies: $k_B T_e \ll \hbar/W \ll \hbar/\tau_D \ll E_F$, with E_F representing the Fermi energy and T_e representing the electron temperature. In this case, the corresponding scattering matrix in the energy domain can be written as²¹

$$b(E) = \int_{-\infty}^{+\infty} \frac{dE'}{2\pi\hbar} S(E - E') a(E'), \quad (2)$$

where $a(E)$ and $b(E)$ represent the electron annihilation operators in the Ohmic contact and the quantum conductor, respectively. The matrix element $S(E - E')$ is only the function of the energy difference $E - E'$, which can be related to the voltage pulse $V(t)$ as

$$S(E - E') = \int_{-\infty}^{+\infty} dt e^{\frac{i}{\hbar}[(E - E')t - e \int^t d\tau V(\tau)]}. \quad (3)$$

Note that for the voltage pulse we considered here, the scattering matrix is symmetric, *i.e.*, $S(E, E') = S(E', E)$, since we have $V(t) = -V(-t)$ from Eq. (1).

It is convenient to write the scattering matrix into the form of the polar decomposition in the energy domain.^{22–24} For the symmetric scattering matrix, the decomposition can be written as²⁰

$$S(E, E') = \sum_k [\psi_k^e(E), \psi_k^h(E)]^* \times \begin{bmatrix} \sqrt{1 - p_k} & i\sqrt{p_k} \\ i\sqrt{p_k} & \sqrt{1 - p_k} \end{bmatrix} \begin{bmatrix} \psi_k^e(E') \\ \psi_k^h(E') \end{bmatrix}, \quad (4)$$

with k being a positive integer and the notation \dots^* denoting the complex conjugation. The quantity p_k is real and lies in the region $[0, 1]$. The two functions $\psi_k^e(E)$ and $\psi_k^h(E)$ are both complex and satisfy: $\psi_k^e(E) = 0$ for $E \leq 0$ and $\psi_k^h(E) = 0$ for $E > 0$.

Given the scattering matrix, one can construct the many-body state of the quantum conductor from the

first-order electronic correlation function via the Bloch-Messiah reduction.²⁰ In doing so, one obtains the many-body state in the zero-temperature limit ($T_e \rightarrow 0$) as

$$|\Psi_b\rangle = \sum_k \left[\sqrt{1-p_k} + i\sqrt{p_k} B_e^\dagger(k) B_h^\dagger(k) \right] |F\rangle, \quad (5)$$

where $|F\rangle$ represents the Fermi sea and $B_e^\dagger(k)[B_h^\dagger(k)]$ represents the creation operator for the electron[hole] component. They can be related to the polar decomposition Eq. (4) as

$$\begin{aligned} B_e^\dagger(k) &= \int_0^{+\infty} \frac{dE}{2\pi\hbar} \psi_k^e(E) a^\dagger(E), \\ B_h^\dagger(k) &= \int_{-\infty}^0 \frac{dE}{2\pi\hbar} \psi_k^h(E) a(E), \end{aligned} \quad (6)$$

This form suggests that only eh pairs are excited in the Fermi sea by the voltage pulses $V(t)$. The quantum state of each pair are characterized by the excitation probability p_k and the one-body wave function of the electron[hole] component $\psi_k^{e[h]}(E)$, which can be solely decided from the polar decomposition of the scattering matrix shown in Eq. (4).

The above equations establish a general relation between the voltage pulse $V(t)$ and the quantum states of the eh pairs. By choosing t_0 as the time unit, the overall shape of the pulse can be characterized by the (dimensionless) width W/t_0 and the flux φ , while the fine structure of the shape is decided by the detailed profile of $V_p(t)$. All these three ingredients can affect the quantum state of the eh pairs.

III. CLASSIFICATION OF THE ELECTRON-HOLE PAIRS

Despite the different profile of $V_p(t)$, we find that the eh pairs can always be classified into two kinds, which can be seen from their excitation probabilities p_k . To demonstrate this, let us consider the case of the Gaussian profile, when $V_p(t)$ has the form

$$V_p(t) = \frac{2\hbar\sqrt{\pi\ln 2}}{e} \frac{\varphi}{W} \exp\left[-\left(\frac{t\sqrt{\ln 2}}{W}\right)^2\right]. \quad (7)$$

A. Excitation probability

We show the typical behavior of the probabilities p_k as functions of the flux φ in Fig. 2(a), corresponding to $W/t_0 = 1/8$.²⁵ One can see that the excitation is dominated by the first five eh pairs ($k = 1-5$). There are two additional eh pairs ($k = 6$ and 7), whose excitation probabilities are much smaller and can only be distinguished from the zoom-in plot shown in Fig. 2(b). The probabilities of the other eh pairs are negligible due to their small probabilities: They are all smaller than 0.002, which cannot be seen even in the zoom-in plot.

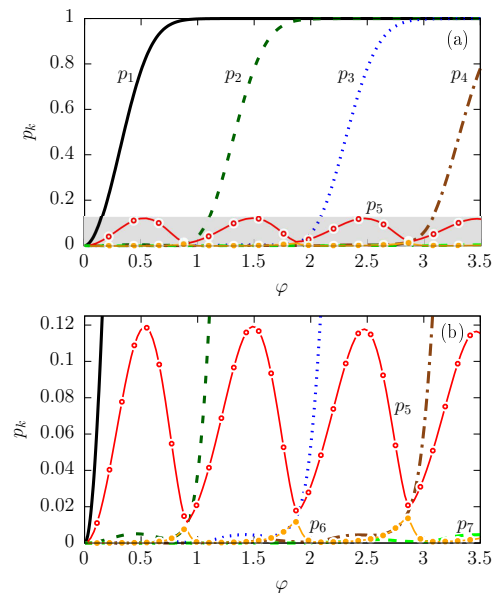


FIG. 2. (Color online) (a) Excitation probabilities as functions of the flux φ in the case of the Gaussian profile, corresponding to the width $W/t_0 = 1/8$. The black solid, green dashed, blue dotted and brown dash-dotted curves correspond to the first four normal eh pairs ($k = 1-4$). The red solid curve with circles corresponds to the first abnormal eh pair ($k = 5$). (b) Zoom-in plot of the grey regime. The orange solid curve with dots corresponds the second abnormal eh pair ($k = 6$), while the bright-green dashed curve corresponds to the fifth normal eh pair ($k = 7$). The minima of the probability p_5 occur at $\varphi = 0.90, 1.88$ and 2.87 ; while the maximums of the probability p_6 occur at $\varphi = 0.89, 1.87$ and 2.85 .

All these eh pairs can be classified into two kinds, whose probabilities exhibit quite different dependence on the flux φ . There are five eh pairs ($k = 1-4$ and 7), which belong to the first kind. The corresponding probability p_k remains quite small when the flux φ is below a certain threshold value. Above the threshold, p_k increases monotonically and saturates to the maximum value 1 when the flux φ is large enough. For example, the probability p_2 (green dashed curve) is kept below 0.04 for φ below the threshold 1.0, which can only be seen clearly from the zoom-in plot Fig. 2(b). Note that in this regime, p_2 can change non-monotonically upon the flux φ . For φ above the threshold 1.0, p_2 increases monotonically. It can reach above 0.99 for $\varphi > 1.87$, as shown in Fig. 2(a). It is worth noting that the similar behavior of the probabilities has been reported in the case of the ac driving.^{20,26} This is easy to be understood, since the voltage pulse $V(t)$ we studied here [see, Fig 1(c)] can be regarded as a single period of ac driving voltage. Due to such similarity in the probabilities, we here refer to the eh pairs of the first kind as “normal” eh pairs.

In contrast, for eh pairs of the second kind ($k = 5$ and 6), the corresponding probabilities undergo oscillations with the flux φ . The probability p_5 exhibits minimums around the point when φ takes integer values, while p_6

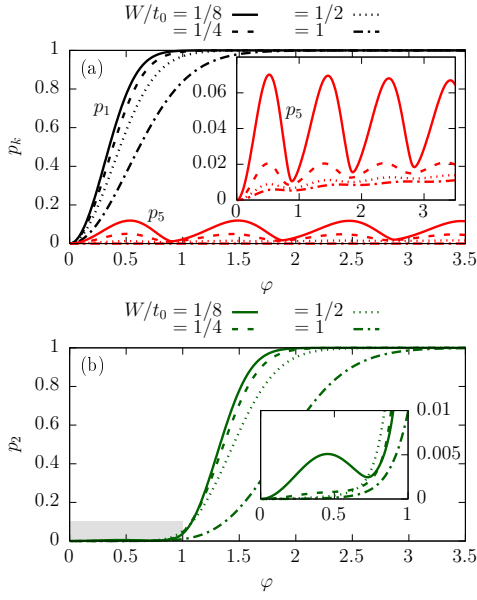


FIG. 3. (Color online) (a) The probabilities p_1 (black curve) and p_5 (red curve) as functions of the flux φ for different pulse width W/t_0 . The detailed behavior of p_5 is shown in the inset. (b) The probability p_2 as functions of the flux φ for different pulse width W/t_0 . The inset shows the zoom-in plot of the grey regime.

tends to exhibit maximums at almost the same positions [see the caption in Fig. 2(b) for the detailed positions]. This kind of eh pairs is absent in the case of the ac driving, hence we here refer to them as “*abnormal*” eh pairs.

One may wonder why the abnormal eh pairs cannot be excited via the ac driving voltage? The main reason is that the width W/t_0 corresponding to a single period of typical ac driving is rather large ($W/t_0 \sim 1$). In this case, the excitation of the abnormal eh pairs is strongly suppressed. To illustrate this, we compare the probabilities p_1 (normal eh pair) and p_5 (abnormal eh pair) as functions of the flux φ for different width W/t_0 in Fig. 3(a). The solid, dashed, dotted and dash-dotted curves correspond to the width $W/t_0 = 1/8, 1/4, 1/2$ and 1 , respectively. One can see that by increasing the width W/t_0 , both the probabilities can be suppressed. However, the suppression for p_1 is relatively weak and becomes marginal for $\varphi > 1.5$. So it can still play an important role even for $W/t_0 = 1$. In contrast, the suppression for p_5 is much more pronounced. For $W/t_0 \geq 1/2$, p_5 is too small and can only be seen clearly from the inset.

Note that the non-monotonically behavior of the normal eh pairs can also be suppressed as the pulse width W/t_0 increasing. This can be seen from Fig. 3(b), where we plot the probability p_2 as functions of the flux φ with different width W/t_0 . By comparing to p_1 shown in Fig. 3(a), one can see that the probability p_2 has a more sensitive dependence on W/t_0 . Moreover, from the inset of Fig. 3(b), one finds that the non-monotonically behavior of p_2 can only be seen for $W/t_0 = 1/8$, as il-

lustrated by the green solid curve. For $W/t_0 \geq 1/4$, p_2 always increases monotonically as φ increasing.

In theory, as the pulse width W/t_0 further decreasing, the abnormal eh pairs can play a more and more important role. In the meantime, the non-monotonically behavior of the normal eh pairs can also be more pronounced. However, it is difficult to realize a well-behaved nanosecond voltage pulse for too small width W/t_0 in practical. Experimentally, one usually stays in the region for $W/t_0 > 0.1$.¹⁵ In this region, the excitation probabilities of the abnormal eh pairs are typically much smaller than the ones of the normal eh pairs. In fact, due to the small probability p_6 [see Fig. 2], the impact of the second abnormal eh pair ($k = 6$) is negligible in most cases and only the first one ($k = 5$) is relevant. In the meantime, the non-monotonically behavior of the normal eh pairs can usually play negligible roles, as the probability of the normal eh pairs are rather small below the threshold.

B. Full counting statistics

Due to the oscillation of the probabilities, it is expected that the abnormal eh pairs can lead to different statistics for pulses with integer and noninteger fluxes. To study this, we calculate the full counting statistics (FCS) $P(N)$ of the eh pairs, corresponding to the probability of exciting N eh pairs over the time interval $[-t_f/2, t_f/2]$. In the limit $t_f \rightarrow +\infty$, the cumulant generating function (CGF) $[e^{S(\chi)} = \sum_N P(N)e^{iN\chi}]$ can be related to the excitation probability p_k as²⁰

$$S(\chi) = \sum_k \ln(1 - p_k + e^{i\chi}p_k). \quad (8)$$

This corresponds to the Poisson binomial distribution, which is typical for non-interacting particles.¹⁰ It allows us to separate the contribution of the abnormal eh pairs from the normal ones, making it easier to study their impacts.

Usually, the FCS are characterized by the mean $N_{ph} = \sum_N P(N)N$, variance $\sigma_{ph}^2 = \sum_N P(N)N^2 - N_{ph}^2$ and high-order cumulants, which can be obtained from derivatives of $S(\chi)$. For the voltage pulse electron source we considered here, there exists an alternative way to characterize the FCS. This is because the CGF in this case can be approximate as

$$S(\chi) \approx \alpha \ln(1 - \bar{p} + e^{i\chi}\bar{p}), \quad (9)$$

corresponding to an effective binomial distribution. The two parameters α and \bar{p} can be determined by requiring the effective binomial distribution has the same mean and variance as the Poisson binomial distribution, *i.e.*,

$$\begin{aligned} \alpha\bar{p} &= N_{ph} = \sum_k p_k, \\ \alpha\bar{p}(1 - \bar{p}) &= \sigma_{ph}^2 = \sum_k p_k(1 - p_k). \end{aligned} \quad (10)$$

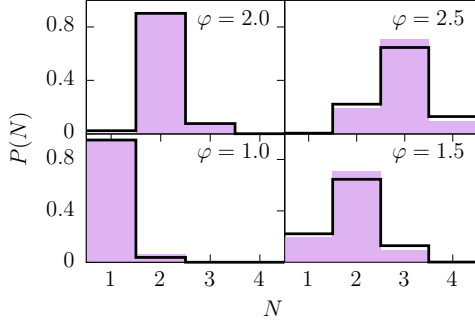


FIG. 4. (Color online) The exact FCS $P(N)$ from Eq. (8) (pink bars) and the FCS from the effective binomial distribution (black curves) with different pulse fluxes $\varphi = 1.0, 1.5, 2.0$ and 2.5 . All the FCS are obtained by using the Gaussian profile with width $W/t_0 = 1/8$.

In Fig. 4, we compare the $P(N)$ from Eq. (8) (pink bars) with the $P(N)$ from Eq. (9) (black curves) in several typical cases, which shows that the effective binomial distribution can offer a good estimation of the overall behavior of the FCS.²⁷

Hence the two parameters α and \bar{p} can be used to characterize the FCS of the eh pairs. They indicate that the voltage pulse can excite effectively α eh pairs with an effective probability \bar{p} , offering an alternative but more intuitive way to interpret the physical meaning of the FCS. In particular, α and \bar{p} can show different behaviors *without* and *with* the contribution of the abnormal eh pairs, from which their impact on the FCS can be seen more clearly.

To see this, let us first concentrate on the parameter α of the effective binomial distribution. We show α as a function of the flux φ *without* and *with* the contribution of the abnormal eh pairs in Fig. 5(a) and (b), respectively. In the figure, different curves correspond to different pulse width W/t_0 . From Fig. 5(a), one can see that, *without* the contribution of the abnormal eh pairs, α can exhibit a sequencing of plateaus. The structure of the plateaus can be seen more clearly from the red solid curve, corresponding to $W/t_0 = 1/8$. This curve shows that the plateaus are quantized at positive integer values $n = 1, 2, 3, \dots$, as indicated by the grey dotted horizontal lines. As φ increasing, α can change from the n th plateau to the next one, whenever φ is large than the corresponding integer n .

The plateaus are pronounced for small width W/t_0 . As W/t_0 increasing, all the plateaus tend to diminish, except for the lowest one. This can be seen by comparing the red solid curve to the black dashed ($W/t_0 = 1/4$), blue dotted ($W/t_0 = 1/2$) and green dash-dotted ($W/t_0 = 1$) ones in Fig. 5(a). For $W/t_0 = 1$, only the lowest plateau preserves, while the other plateau are merged into a smooth rise with small ripples.

The abnormal eh pairs can induce a derivation of α from the plateaus, as shown in Fig. 5(b). Such deriva-

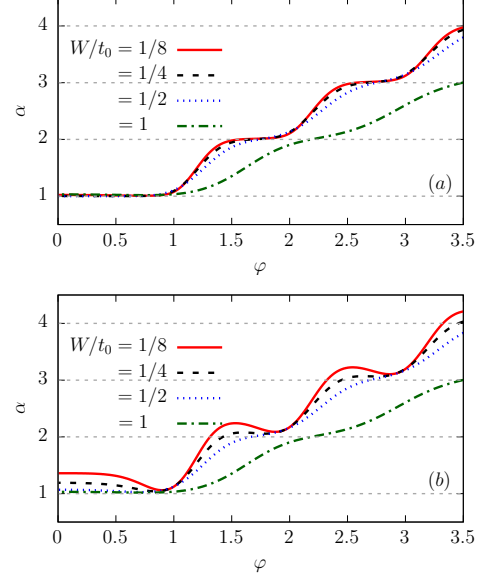


FIG. 5. (Color online) The parameter α of the effective binomial distribution (a) *without* and (b) *with* the contribution of the abnormal eh pairs. The red solid, black dashed, blue dotted and green dash-dotted curves correspond to the width $W/t_0 = 1/8, 1/4, 1/2$ and 1 , respectively.

tion can be seen more clearly by comparing the red solid curves in Fig. 5(a) and (b), corresponding to $W/t_0 = 1/8$. By comparing the two curves, one can see that the derivation is mainly due to the enhancement of α at noninteger fluxes. By further comparing them to the excitation probabilities in Fig. 2, one can see that such enhancement can be attributed to the contribution of the probability p_5 : The enhancement is strong whenever p_5 tends to exhibit a maximum. The only exception occurs around the point $\varphi = 0$, where the enhancement of α is rather strong, while the probability p_5 is dropping to zero. The main reason of such exception is that: The excitation probabilities of the normal eh pairs also drop rapidly to zero as $\varphi \rightarrow 0$. This makes p_5 can still lead to a significant contribution to the FCS at this point.

As the width W/t_0 increasing, p_5 decreases rapidly, as we have shown in Fig. 3. Accordingly, the enhancement of α becomes less and less pronounced, as can be seen in Fig. 5(b). For $W/t_0 = 1/2$ (blue dotted curve), the enhancement is too weak so that the derivation of α from the plateaus can no longer be observed in the figure.

While the abnormal eh pairs can affect the behavior of α distinctly, their impact on \bar{p} is much less pronounced. In fact, the probability \bar{p} *without* and *with* the contribution of the abnormal eh pairs show quite similar oscillations, which can be seen from Fig. 6(a) and (b).

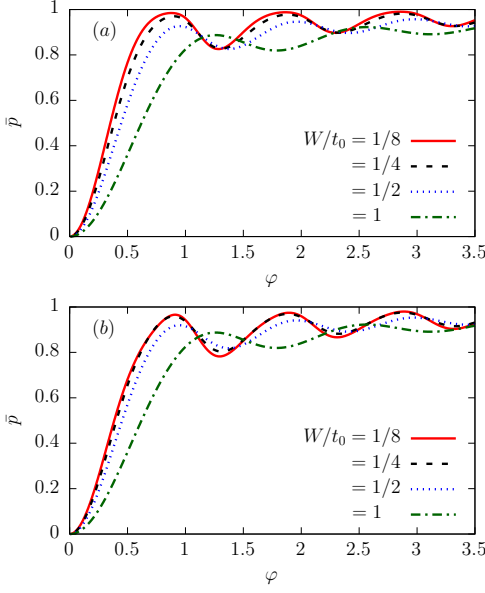


FIG. 6. (Color online) The parameter \bar{p} of the effective binomial distribution (a) *without* and (b) *with* the contribution of the abnormal eh pairs. The red solid, black dashed, blue dotted and green dash-dotted curves correspond to the width $W/t_0 = 1/8, 1/4, 1/2$ and 1 , respectively.

IV. PULSE SHAPE DEPENDENCE

Although the above results are obtained by using the voltage pulse with the Gaussian profile, the classification of the normal and abnormal eh pairs are quite general and can be seen for pulses with different profiles. We have checked the excitation probabilities of the Square, Triangular and Parabolic profiles, which show quite similar behaviors as the ones of the Gaussian profile [see Appendix A for details]. Among various profiles, of particular interest is the Lorentzian profile, which plays an important role in the study of levitons. One may wonder what happens to the abnormal eh pairs when the profile of the pulse is tuned to be the Lorentzian. To demonstrate this, let us consider the case of a mixed Lorentzian-Gaussian profile, when the corresponding $V_p(t)$ has the form

$$V_p(t) = r \frac{\hbar}{e} \frac{2W\varphi}{W^2 + t^2} + (1-r) \frac{\sqrt{2\pi}\hbar}{e} \frac{\varphi}{W} \exp\left[-\left(\frac{t\sqrt{\ln 2}}{W}\right)^2\right]. \quad (11)$$

Here, the first term represents the Lorentzian profile, while the second term represents the Gaussian profile. The parameter r characterizes the degree of mixture between the two profiles. By increasing r from 0 to 1, the profile can evolve continuously from the Gaussian to the Lorentzian.

We show the typical behavior of the excitation probabilities as functions of the flux φ in Fig. 7, corresponding to $r = 0.4$ and $W/t_0 = 1/8$. Comparing to Fig. 2 (corre-

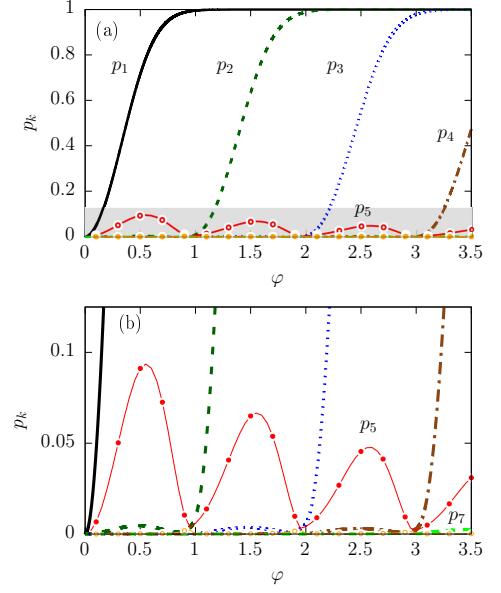


FIG. 7. (Color online) The same as Fig. 2, but with the mixed Lorentzian-Gaussian profile, where $r = 0.4$ and $W/t_0 = 1/8$. Note that the probability p_6 of the second abnormal eh pair becomes too small to be seen, even in the zoom-in plot shown in (b).

sponding to $r = 0.0$), one can see that the probabilities exhibit qualitatively similar behaviors, from which one can identify the normal and abnormal eh pairs following the same procedure introduced in the previous section. Note that in this case, all the probabilities are suppressed compared to the case of the Gaussian profile. For the normal eh pairs, the suppression is modest: One can still find five normal ($k = 1-4$ and 7) eh pairs in this case, whose excitation probabilities exhibit quite similar features as the ones of the Gaussian profile. In contrast, the suppression is more pronounced for the abnormal eh pairs. Due to the suppression, only the excitation probability p_5 can be identified, corresponding to the first abnormal eh pair. The probability p_6 of the second abnormal eh pair becomes too small to be observable, even in the zoom-in plot shown in Fig. 7(b).

The suppression of the probability of the abnormal eh pairs is particular pronounced when the flux φ takes integer values. To clarify this, we show the probability p_5 with different mixture parameters r in Fig. 8(a), corresponding to the first abnormal eh pair. One can see that the oscillation of p_5 undergoes a damping oscillation with the flux φ . The damping becomes more and more strong as r increasing. In the meantime, the minimums of the oscillation move toward the points where φ takes integer values. As r reaching 1.0, all the minimums drop to zero at these points, as illustrated by the red solid curve in the figure. This feature indicates that the excitation of the abnormal eh pairs is absent for the Lorentzian-shape pulse with integer fluxes.

The suppression of the probabilities at integer fluxes

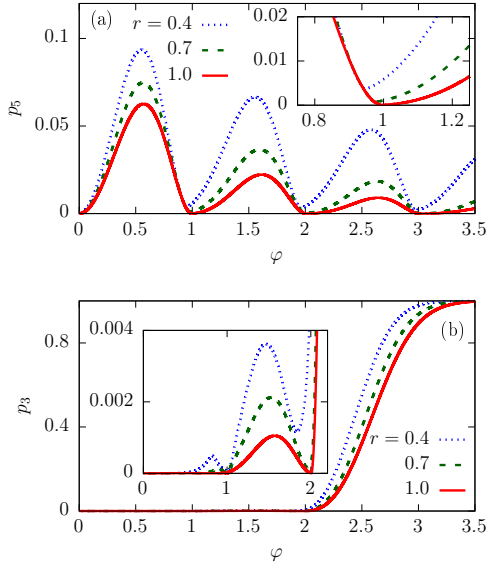


FIG. 8. (Color online) (a) The probability p_5 as functions of the flux φ with different mixture parameters r . The detailed behavior of p_5 around $\varphi = 1$ is shown in the inset. (b) The probability p_3 as functions of the flux φ with different mixture parameters r . The detailed behavior of p_3 below the threshold 2.0 is shown in the inset.

can also be seen from the normal eh pairs, but in a more subtle way. To demonstrate this, we plot the probability p_3 with different mixture parameters r in Fig. 8(b), corresponding to the third normal eh pair. For $r = 0.4$ (blue dotted curve), one can see that p_3 is kept smaller than 0.004 below the threshold $\varphi = 2.0$, which can be seen more clearly from the inset. For $\varphi > 2.0$, p_3 increase monotonically and can reach almost the maximum value 1 when $\varphi = 3.5$. By increasing the mixture parameter r from 0.4 to 1.0, p_3 can be suppressed to zero for $\varphi = 1.0$ and 2.0, which are below the threshold [see the inset]. For $\varphi > 2.0$, the suppression is absent and the probabilities p_3 for different r show quite similar behaviors, as shown in the main panel of the Fig. 8(b).

V. SUMMARY

In this paper, we study the quantum states of the eh pairs excited in a voltage-pulse-driven quantum conductor. By using the Gaussian-shaped pulse as an example, we show that the eh pairs can always be classified into the normal and abnormal eh pairs, whose excitation probabilities exhibit different dependence on the flux of the pulse φ . For the normal eh pairs, the probabilities increase nearly monotonically with the flux. They can reach the maximum value 1 when the flux is strong enough. In contrast, the excitation probabilities of the abnormal eh pairs undergo oscillation with the flux. These pairs can only be excited for pulses with small

width. In practical cases, only the first abnormal eh pair is relevant.

We find that the abnormal eh pairs can lead to different features in the FCS of the eh pairs for pulses with integer and noninteger fluxes. This features can be better seen from the effective binomial distribution, whose CGF has the form $S(\chi) = \alpha \ln(1 - \bar{p} + e^{i\chi}\bar{p})$. Without the contribution of the abnormal eh pairs, the parameter α exhibits a sequencing of plateaus. The abnormal eh pairs can lead to a derivation from these plateaus, which can be treated as a signature of the abnormal eh pairs.

We also find that the classification of the normal and abnormal eh pairs is quite general and can be found for pulses with different profiles. In particular, as the profile of the pulse evolves from the Gaussian to the Lorentzian, we show that the excitation of the abnormal eh pairs can be totally suppressed when the pulse flux φ takes integer values.

ACKNOWLEDGMENTS

This work was supported by National Key Basic Research Program of China under Grant No. 2016YFF0200403.

Appendix A: Excitation probabilities of other profiles

In this appendix, we present the excitation probabilities for the Square, Triangular and Parabolic profiles:

Square profile:

$$V_p(t) = \begin{cases} \frac{\pi\hbar}{e} \frac{\varphi}{W} & , \quad |t| < W \\ 0 & , \quad \text{otherwise.} \end{cases} \quad (\text{A1})$$

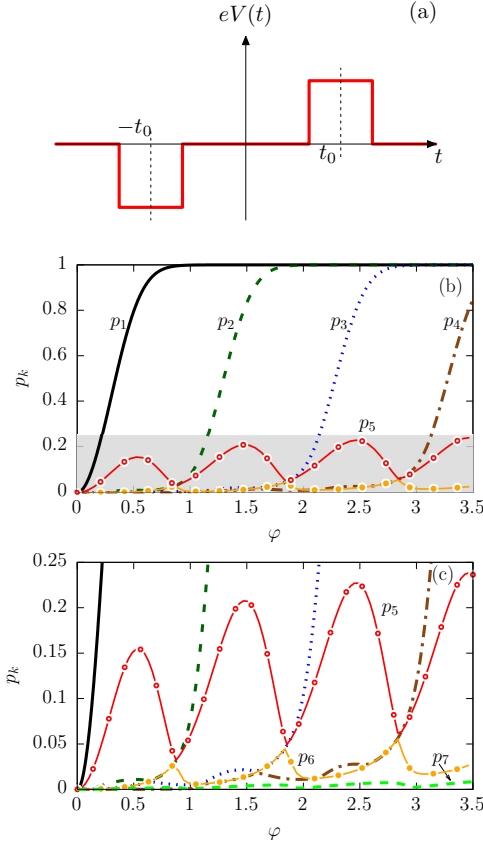


FIG. 9. (Color online) (a) Schematic of the Square-profile pulse in time-domain. (b) Excitation probabilities as functions of the flux φ , with the width $W/t_0 = 1/8$. (c) Zoom-in plot of the grey regime.

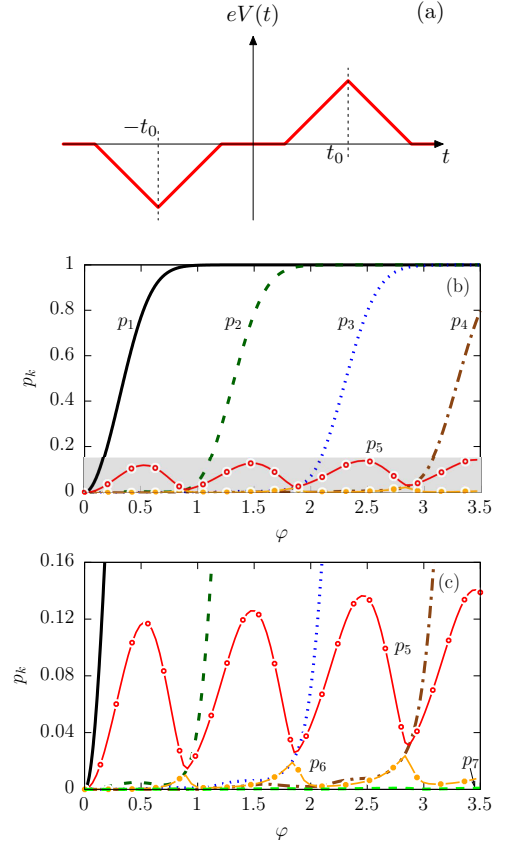


FIG. 10. (Color online) (a) Schematic of the Triangular-profile pulse in time-domain. (b) Excitation probabilities as functions of the flux φ , with the width $W/t_0 = 1/8$. (c) Zoom-in plot of the grey regime.

Triangular profile:

$$V_p(t) = \begin{cases} \frac{\pi\hbar}{2e} \frac{\varphi}{W^2} (2W - |t|) & , \quad |t| < 2W \\ 0 & , \quad \text{otherwise.} \end{cases} \quad (\text{A2})$$

Parabolic profile:

$$V_p(t) = \begin{cases} \frac{3\pi\hbar}{2\sqrt{2}e} \frac{\varphi}{W} (1 - \frac{t^2}{2W^2}) & , \quad |t| < \sqrt{2}W \\ 0 & , \quad \text{otherwise.} \end{cases} \quad (\text{A3})$$

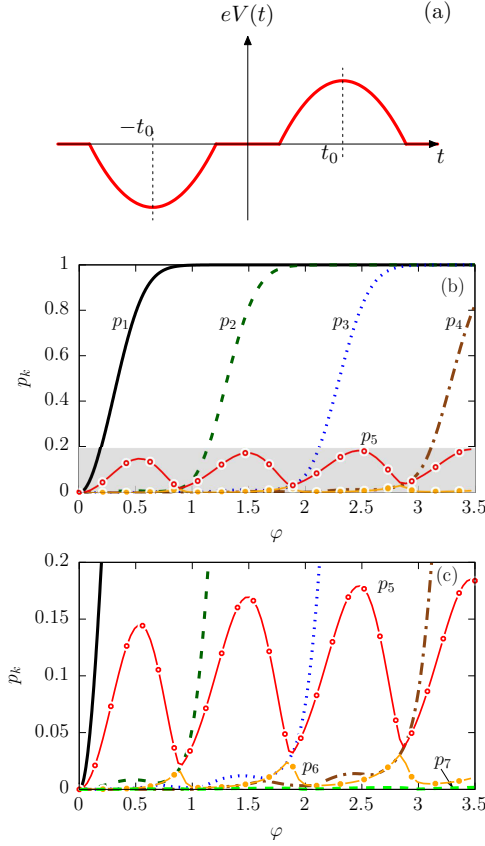


FIG. 11. (Color online) (a) Schematic of the Parabolic-profile pulse in time-domain. (b) Excitation probabilities as functions of the flux φ , with the width $W/t_0 = 1/8$. (c) Zoom-in plot of the grey regime.

Appendix B: Effective binomial distribution of other profiles

In this appendix, we show the parameters α and \bar{p} of the effective binomial distribution *without* and *with* the contribution of the abnormal eh pairs for different profiles.

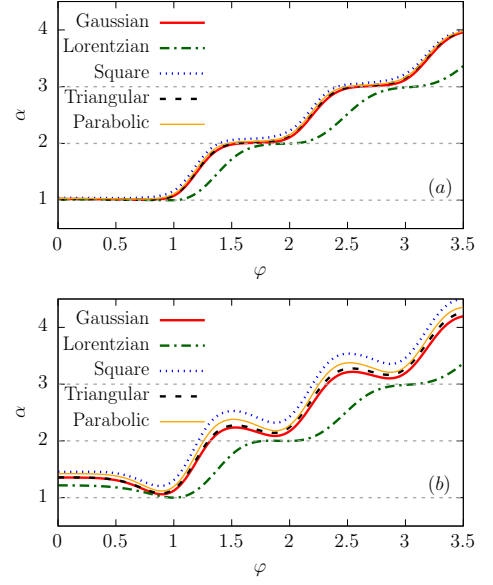


FIG. 12. (Color online) The parameter α of the effective binomial distribution (a) *without* and (b) *with* the contribution of the abnormal eh pairs. The red solid, green dash-dotted, blue dotted, black dashed, and orange thin solid curves correspond to the Gaussian, Lorentzian, Square, Triangular and Parabolic profiles, respectively.

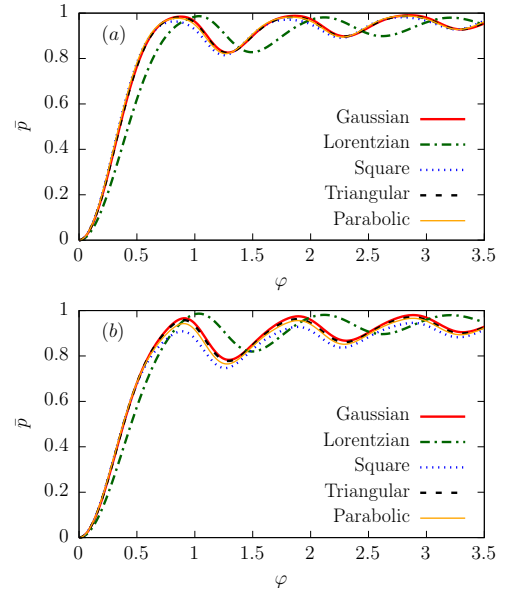


FIG. 13. (Color online) The parameter \bar{p} of the effective binomial distribution (a) *without* and (b) *with* the contribution of the abnormal eh pairs. The red solid, green dash-dotted, blue dotted, black dashed, and orange solid curves correspond to the Gaussian, Lorentzian, Square, Triangular, Parabolic profiles respectively.

-
- * Author to whom correspondence should be addressed; yin80@scu.edu.cn.
- ¹ J. Keeling, I. Klich, and L. S. Levitov, Phys. Rev. Lett. **97**, 116403 (2006).
 - ² G. Fève, A. Mahé, J. M. Berroir, T. Kontos, B. Plaçais, D. C. Glattli, A. Cavanna, B. Etienne, and Y. Jin, Science **316**, 1169 (2007).
 - ³ J. Keeling, A. V. Shytov, and L. S. Levitov, Phys. Rev. Lett. **101**, 196404 (2008).
 - ⁴ A. Mahé, F. D. Parmentier, E. Bocquillon, J.-M. Berroir, D. C. Glattli, T. Kontos, B. Plaçais, G. Fève, A. Cavanna, and Y. Jin, Phys. Rev. B **82**, 201309 (2010).
 - ⁵ J. D. Fletcher, P. See, H. Howe, M. Pepper, S. P. Giblin, J. P. Griffiths, G. A. C. Jones, I. Farrer, D. A. Ritchie, T. J. B. M. Janssen, and M. Kataoka, Phys. Rev. Lett. **111**, 216807 (2013).
 - ⁶ C. Bäuerle, D. C. Glattli, T. Meunier, F. Portier, P. Roche, P. Roulleau, S. Takada, and X. Waintal, Reports on Progress in Physics **81**, 056503 (2018).
 - ⁷ L. D. Landau, JETP **3**, 920 (1957).
 - ⁸ D. Pines and P. Nozières, *The Theory of Quantum Liquids* (CRC Press, 2018).
 - ⁹ D. C. Glattli and P. S. Roulleau, phys. stat. sol. (b) **254**, 1600650 (2016).
 - ¹⁰ L. S. Levitov, H. Lee, and G. B. Lesovik, J. Math. Phys. **37**, 4845 (1996).
 - ¹¹ M. Vanević, Y. V. Nazarov, and W. Belzig, Physical Review Letters **99**, 076601 (2007).
 - ¹² D. A. Ivanov, H. W. Lee, and L. S. Levitov, Physical Review B **56**, 6839 (1997).
 - ¹³ J. Dubois, T. Jullien, F. Portier, P. Roche, A. Cavanna, Y. Jin, W. Wegscheider, P. Roulleau, and D. C. Glattli, Nature **502**, 659 (2013).
 - ¹⁴ E. Bocquillon, V. Freulon, F. D. Parmentier, J.-M. Berroir, B. Plaçais, C. Wahl, J. Rech, T. Jonckheere, T. Martin, C. Grenier, D. Ferraro, P. Degiovanni, and G. Fève, Ann. Phys. **526**, 1 (2014).
 - ¹⁵ J. Dubois, T. Jullien, C. Grenier, P. Degiovanni, P. Roulleau, and D. C. Glattli, Physical Review B **88**, 085301 (2013).
 - ¹⁶ D. C. Glattli and P. Roulleau, Physical Review B **97**, 125407 (2018).
 - ¹⁷ P. P. Hofer and C. Flindt, Physical Review B **90**, 235416 (2014).
 - ¹⁸ M. Moskalets, Phys. Rev. Lett. **117**, 046801 (2016).
 - ¹⁹ M. Vanević, J. Gabelli, W. Belzig, and B. Reulet, Physical Review B **93**, 041416 (2016).
 - ²⁰ Y. Yin, Journal of Physics: Condensed Matter **31**, 245301 (2019).
 - ²¹ C. W. J. Beenakker, M. Titov, and B. Trauzettel, Physical Review Letters **94**, 186804 (2005).
 - ²² C. W. J. Beenakker, Rev. Mod. Phys. **69**, 731 (1997).
 - ²³ R. A. Jalabert, *New Directions in Quantum Chaos*, edited by G. Casati, I. Guarneri, and U. Smilansky (IOS Press, Amsterdam, 2000).
 - ²⁴ P. A. Mello and N. Kumar, *Quantum Transport in Mesoscopic Systems* (Oxford University Press, Oxford, UK, 2004).
 - ²⁵ The eh pairs can be distinguished via their one-body wave function. In this paper, we assume that the wave function of each eh pair evolves continuously with the flux φ , i.e., $\lim_{\delta\varphi \rightarrow 0} \int dE [\psi_k^{e(h)}(E; \varphi)]^* \psi_{k'}^{e(h)}(E; \varphi + \delta\varphi) = \delta_{k-k'}$. This allows us to study the φ -dependence of the probability for each eh pair individually.
 - ²⁶ M. Vanević, Y. V. Nazarov, and W. Belzig, Physical Review B **78**, 245308 (2008).
 - ²⁷ Strictly speaking, the effective binomial distribution Eq. (9) cannot give a positive-defined $P(N)$ via the usual formula $P(N) = \int_{-\pi}^{\pi} \frac{d\chi}{2\pi} e^{S(\chi) - iN\chi}$, when the parameter α is not an integer. Here the FCS $P(N)$ corresponding to the effective binomial distribution is obtained via the saddle point approximation.
 - ²⁸ G. Gasse, L. Spietz, C. Lupien, and B. Reulet, Physical Review B **88**, 241402 (2013).